

# Deep Pulse-Signal Magnification for remote heart rate estimation in compressed videos

Joaquim Comas<sup>1</sup>, Adrià Ruiz<sup>2</sup>, Federico Sukno<sup>1</sup>

<sup>1</sup> Department of Information and Communication Technologies, Pompeu Fabra University, Barcelona, Spain

<sup>2</sup> Seedtag, Madrid, Spain

**Abstract**—Recent advancements in data-driven approaches for remote photoplethysmography (rPPG) have significantly improved the accuracy of remote heart rate estimation. However, the performance of such approaches worsens considerably under video compression, which is nevertheless necessary to store and transmit video data efficiently. In this paper, we present a novel approach to address the impact of video compression on rPPG estimation, which leverages a pulse-signal magnification transformation to adapt compressed videos to an uncompressed data domain in which the rPPG signal is magnified. We validate the effectiveness of our model by exhaustive evaluations on two publicly available datasets, UCLA-rPPG and UBFC-rPPG, employing both intra- and cross-database performance at several compression rates. Additionally, we assess the robustness of our approach on two additional highly compressed and widely-used datasets, MAHNOB-HCI and COHFACE, which reveal outstanding heart rate estimation results.

**Index Terms**—Remote photoplethysmography (rPPG), deep learning, remote heart rate (HR) measurement, video compression.

## I. INTRODUCTION

Recently, the research community has shown increasing interest in the camera-based measurement of human physiological signals. These vital signs, including heart rate (HR), heart rate variability (HRV), respiration rate (RR), oxygen saturation (SpO<sub>2</sub>), and blood volume pulse (BVP) are essential for evaluating individuals' physical and mental state and have numerous potential applications [1], [24], [43]. The advancements in multimedia technology have made many of these potential applications feasible, and have significantly impacted various industries such as education, entertainment, advertising, and healthcare. Thanks to current network connections, smartphones, and other multimedia devices, video content can be accessed or shared effortlessly. Nevertheless, in practical scenarios, the transmission of video content would not be viable without the use of video compression.

While significant progress has been made in remote physiological signal sensing, its application to compressed videos remains challenging. McDuff et al. [30] were among the first to demonstrate the impact of video compression, noting a significant reduction in the rPPG signal-to-noise ratio (SNR), even before human observers perceive a decrease in visual quality. Thus, it was found that even mild compression affects the recovery of the rPPG signal and, through this, the accuracy of derived estimates, such as HR or RR.

Several other works [3], [12], [13], [34] have later highlighted additional effects of video compression on automatic

rPPG analysis, such as the effect of video resolution [49], the heterogeneous impact of compression for different color channels [68], or the greater impact of temporal compression with respect to chroma and spatial compression on the quality of the recovered rPPG signal [42]. More details on these and other studies about the impact of video compression can be found in Section II-C.

Unfortunately, to date, rather few solutions have addressed the challenges of video compression in rPPG estimation. They can broadly be divided into three categories: 1) methods that propose to modify the recording conditions or the encoding algorithm [67], [68]; 2) methods that propose to avoid a mismatch between the compression rates of training and test sets [34], [36]; 3) methods that try to reverse the damage introduced by the compressor [63] (details in Section II-D).

In practice, the first category is of limited scope because it only applies to scenarios where videos are recorded specifically for rPPG estimation purposes. The second category is more widely applicable since it only requires finding a training dataset that matches the compression of the data being targeted; however, its success has been modest, yielding results that are still largely affected by the amount of compression [34]. Thus, the most promising path so far has been the third category, where the most relevant approach was presented by Yu et al. [63], based on an enhancement generator (STVEN) cascaded with a spatiotemporal convolutional network (rPPGNet) to recover the rPPG signal. The enhancement generator is framed within the idea of video quality enhancement (VQE) [9], [65], which requires significant computational resources due to the large amount of data involved in restoring the high-frequency details lost due to video compression. Nevertheless, this is mainly due to the tendency of VQE methods to prioritize visual quality enhancement, which, as we will show, is not strictly needed to recover the rPPG signal.

### A. Contribution

In this work, we propose a novel deep learning framework to mitigate the impact of video compression on rPPG recovery that departs from the objective of Visual Quality Enhancement and focuses, instead, on enhancing only the information required to allow proper recovery of the rPPG signal. To this end, we present a training methodology involving two deep neural networks: (i) The rPPG estimator network, trained on uncompressed videos, that attempts to recover the rPPG signal. (ii) The Pulse-Signal Magnification network (PSMN), that

adapts compressed facial videos to a video domain in which the effects of the blood volume pulse are amplified, yielding a magnified pulse-signal and making possible the rPPG extraction even in highly compressed scenarios. We propose and validate a two-stage optimization procedure for both networks, in which the rPPG estimator acts as a regularizer to facilitate training of the PSMN, considerably improving its performance and yielding physiologically meaningful transformations.

We provide extensive experiments of our approach, demonstrating its robustness and generalization through intra- and cross-dataset evaluation on 4 publicly available datasets: 2 uncompressed ones, UCLA-rPPG and UBFC-rPPG, and 2 highly compressed ones, MAHNOB-HCI and COHFACE.

The remainder of this paper is organized as follows: firstly, in Section II, we conduct a comprehensive review of the effects of video compression on rPPG estimation, the available solutions, and the prevalence of video compression in existing rPPG datasets. The proposed approach is presented in Section III, while experimental results are provided in Section IV. Section V summarizes our findings and conclusions.

## II. RELATED WORK

### A. Camera-based Physiological measurement

Since Takano et al. [52] and Verkruysse et al. [56] showed the feasibility of measuring HR remotely from facial videos, many researchers have proposed different methods to recover physiological data. Among them, some works consider regions of interest using techniques such as Blind Source Separation [20], [40], [41], Normalized Least Mean Squares [23] or self-adaptive matrix completion [55]. In contrast, others rely on the skin optical reflection model by projecting all RGB skin pixel channels into an optimized subspace [8], [57], [58].

Later on, deep learning methods [19], [27], [35], [39], [50], [63] have outperformed conventional methods and achieved state-of-the-art performance in estimating vital signs from facial videos. Some of these methods leverage prior knowledge from traditional methods and combine it with Convolutional Neural Networks (CNNs) to exploit more sophisticated features [31], [33], [46]. Some recent works [19], [26] have explored unsupervised approaches using meta-learning, showing improved generalization in out-of-distribution cases. On the other hand, other researchers have aimed at fully end-to-end approaches [4], [39], [62] using facial videos as input to directly predict the rPPG signal. Attention-based models have recently gained traction in end-to-end approaches, with transformer-based models like Physformer [64] and Efficient-Phys [25] leading the way in leveraging long-range spatiotemporal features. Nevertheless, they have not yet demonstrated a significant performance advantage over CNN-based models [25].

### B. Video-compression in existing rPPG datasets

Several datasets have been collected to advance the research on camera-based physiological sensing, addressing factors such as head movements, illumination conditions, and facial skin diversity. However, until recently, most of them were recorded in compressed video formats [14], [45], [66], which has been

found to negatively impact the performance of rPPG systems (see Section II-C). Thus, a few uncompressed datasets have recently emerged [2], [10], [51], although not all of them are available to the public and have limited sample sizes, making it challenging to propose effective solutions, especially if they are based on deep learning.

Table I summarizes existing rPPG datasets and highlights video compression details, including format, camera specifications, and approximate video quality in terms of bitrate<sup>1</sup>. Although we can distinguish different content formats in the existing rPPG datasets, the majority of them are stored using three standard compression codecs: MPEG-4 Video Part 2 (MPEG-4), Advanced Video Coding (H.264) and Motion JPEG (MJPG).

The most popular standards in Table I are MPEG-4 and H.264, both based on block-wise motion compensation. H.264 is an improved version of MPEG-4, providing better compression due to variable block-size segmentation, optimal discrete cosine transform (DCT), and enhanced inter-frame prediction. While H.264 is the most common format, MPEG-4 is used in some datasets, including COHFACE [14], OBF [22], and CMU [7]. VIPL-HR [32] and UBFC-Phys [44] use the MJPG codec, which compresses each frame individually using JPEG compression, minimizing inter-frame compression's impact on HR estimation [32]. However, the JPEG quantization stage can also be challenging for rPPG solutions.

In contrast, uncompressed datasets have more diversity regarding codec format, with some storing raw data in image files using lossless formats such as PNG, BMP, or Bayer format (e.g., PURE [51], or MR-NIRP [28]), and others using uncompressed video formats, including YUV420, RV32, and RGBA format (e.g., ECG-Fitness [50] or UBFC-rPPG [2]).

Regarding video quality, there are significant average bitrate differences between datasets. For example, UCLA-rPPG [59] has 295 Mb/s while COHFACE [14] has just 0.250 Mb/s. In this case, both datasets use the same camera resolution, but the effects of video compression yield a notable difference in video quality. As noted by Špetlík et al. [49], the encoding standard alone does not determine video quality but other factors, such as the pixel format or the camera resolution, must also be considered in the bitrate computation. For example, the VicarPPG and MAHNOB-HCI datasets use H.264 encoding but with different camera settings, resulting in highly different average bitrates. VicarPPG has a bitrate of 34 Mb/s, while MAHNOB-HCI has a bitrate of 4.20 Mb/s. This means that MAHNOB-HCI has approximately 8.5 times lower quality than VicarPPG.

### C. Influence of video compression on rPPG estimation

Video compression techniques optimize visual quality by removing information imperceptible to the human eye. However, the effects of heart beating on the skin are also imperceptible to the human eye and compression algorithms often remove subtle color variations that are important for inferring rPPG signals. Hanfland et al. [13] were the first to show the

<sup>1</sup>To collect the video information from the different datasets, we contacted the authors of each dataset and utilized the open-source FFmpeg ffprobe tool: <https://ffmpeg.org/ffprobe.html>

TABLE I: Summary of the existing camera-based physiological signal sensing databases and its specifications.

Dataset	Year	Publicly available	Camera Settings	Average Bitrate	Data Format	Subjects	Videos	Signal acquisition
MAHNOB-HCI [45]	2011	Yes	RGB camera, 780x580, 61 Hz	4.20 Mb/s	H.264	27	527	ECG, GSR, RF, ST, EEG
AFRL [10]	2014	No	RGB camera, 658x492, 30 Hz	310 Mb/s	Raw (Bayer)	25	300	ECG, BVP
PURE [51]	2014	Yes	RGB camera, 640x480, 30 Hz	222 Mb/s	Raw (PNG)	10	59	PPG, SpO2
VicarPPG [53]	2014	Yes	Webcam, 720x1280, 30 Hz	34 Mb/s	H.264	10	20	PPG
BP4D [66]	2016	No	Webcam, 1040x1392, 25 Hz	3.5 Mb/s	H.264	140	1400	PPG, RF, HR, EDA
COHFACE [14]	2017	Yes	Webcam, 640x480, 20 Hz	0.25 Mb/s	MPEG-4	40	160	PPG, RF
UBFC-rPPG [2]	2017	Yes	Webcam, 640x480, 30 Hz	215 Mb/s	Raw (RV24)	42	42	HR, PPG
OBF [22]	2018	No	RGB/NIR camera, 1920x1080, 60 Hz	20 Mb/s	MPEG-4	106	212	ECG, RF, PPG
ECG-Fitness [50]	2018	Yes	Webcam, 1920x1080, 30 Hz	745 Mb/s	Raw (YUV420)	17	204	ECG
MR-NIRP [28]	2018	Yes	RGB/NIR camera, 640 × 640, 30 Hz	590 Mb/s	Raw (Bayer)	18	37	PPG
PFV [15]	2020	Yes	Webcam, 1280x720, 50Hz	10 Mb/s	H.264	13	85	HR
VIPL-HR [33]	2020	Yes	RGB/NIR camera, 960x720, 640x480, 25-30 Hz	5.15 Mb/s	MJPEG	107	3130	HR, SpO2, PPG
MOLI-PPG [39]	2020	No	Webcam/RGB camera, 1280x720, 1920x720, 25-50 Hz	Unknown	Raw (BMP)	30	229	PPG
VicarPPG-2 [12]	2020	Yes	Webcam, 1280x720, 60 Hz	16.5 Mb/s	H.264	10	40	PPG, ECG
CMU [7]	2021	Yes	Smartphone, 25x25, 15 Hz	0.145 Mb/s	MPEG-4	140	140	HR
CameraHRV [37]	2021	Yes	RGB camera, 1920x1200, 30 Hz	1659 Mb/s	Raw (Bayer)	14	60	PPG
UBFC-Phys [44]	2021	Yes	RGB camera, 1024x1024, 35 Hz	225 Mb/s	MJPEG	56	168	PPG, EDA
DDPM [48]	2021	Yes	RGB/NIR camera, 1920 × 1080, 90 Hz	950 Mb/s	H.264 <sup>2</sup>	86	86	PPG, SpO2, HR
UCLA-rPPG [59]	2022	Yes	RGB camera, 640x480, 30 Hz	295 Mb/s	Raw (RGBA)	98	489	PPG, HR

influence of video compression on rPPG signal extraction. They compressed raw videos using Motion JPEG, MPEG-4, and Motion JPEG 2000 codecs and computed the time-domain correlation between the videos and extracted signals. A key conclusion from their work is that the rPPG signal is still present in the compressed videos, although they also find that its overall quality is altered by the compression.

McDuff et al. [30] analyzed the impact of video compression on rPPG signal quality by testing two compression standards, H.264 and H.265, at different compression rates. They found noticeable degradation of the rPPG signal even under mild compression and concluded that only videos with a bit rate of at least 10 Mb/s maintained an rPPG signal with reasonable SNR. They also found H.265 to outperform H.264, especially for videos with large movement variations. Similarly to McDuff et al., [30], Cerina et al. [3] analyzed the impact of frame rate and video compression on remote pulse-rate variability (PRV) using a lossless (FFV1) and lossy format (H.264) at two compression rates. They observed a notable trade-off between PRV quality and storage size in FFV1 format, while H.264 showed higher degradation in PRV, depending on peak detection accuracy.

Other studies have further explored the impact of video encoding on camera physiological measurements. Špetlík et al. [49] identified errors in the acquisition stage and conducted an experiment similar to [30] to demonstrate the degradation of

rPPG signal SNR at various compression rates using H.264 encoding. They found that lower resolutions had a higher impact on the recovered signal SNR and emphasized the negative effects of chroma subsampling, common in web camera hardware settings. Rapczynski et al. [42] analyzed the effects of different factors in video compression, finding that inter-frame compression was more damaging than intra-frame compression or chroma subsampling. Zhao et al. [68] found that high compression levels affect blue and red color channels the most in terms of amplitude degradation, high-frequency noise, and trace discontinuity. Nowara et al. [36] extended the study of video compression on rPPG recovery to evaluate the effects of large head motion and skin color diversity.

Other works have investigated the impact of video compression on the development of rPPG datasets. Niu et al. [32] compressed the raw data using five different video codecs: MJPG, FMP4, DIVX, PIM1, and H264, and evaluated the accuracy of HR estimation. They found that the MJPG codec provided a reasonable balance between data compression and preservation of rPPG signals. In contrast, Gudi et al. [12] explored the trade-off between rPPG accuracy and video size/bitrate in the PURE dataset. They tested several lossy (VP9, H.264, H.265, MJPG, MPEG-4) and lossless (FFV1, HuffYUV) video codecs at multiple bitrates. They concluded that H.265 and FFV1 were the most efficient codecs for preserving rPPG accuracy and storage, respectively.

Our findings, discussed in Section IV-C2, align with these prior studies that highlight the negative effects of video

<sup>2</sup>The original camera pixel format was YUV422P format, but it was compressed in a lossless H.264 using a Constant Rate Factor (CRF) of 0

compression on the retrieval of rPPG signals. Moreover, in addition to validating these observations, we introduce a novel approach in Section III to mitigate the adverse effects induced by video compression.

#### D. rPPG solutions for compressed facial videos

While several studies have evaluated the effects of compression on rPPG measurements, very few have proposed solutions to mitigate such effects. Zhao et al. [68] developed a single-channel pulse extraction method that only considers the green channel, as they found that it is the least affected one by compression artefacts. However, ignoring the other channels leads to suboptimal estimations because important rPPG information is neglected. Another solution proposed by Zhao et al. [67] involved designing a new video codec that compresses regions not involved in rPPG extraction, but this approach is not practical for already compressed videos and is challenging to standardize across all multimedia content.

Data-driven solutions have also been explored. McDuff [29] introduced a deep super-resolution preprocessing step to restore high-frequency spatial details from low-resolution or intra-frame (spatial) compressed facial videos. Thus, this method does not consider the adverse effects of inter-frame (temporal) compression. In contrast, Nowara et al. [34], [36] demonstrated that models trained on videos with the same compression level as the test set achieve better performance with respect to mismatched train-test compression; however, this requires knowledge of the compression rate of the testing videos and appropriately matched training data.

Finally, Yu et al. [63] presented the first enhancement method to deal with temporal compression using a video-to-video generator called STVEN and an rPPG estimator called rPPGNet. They employed a three-stage training process and multiple objective loss functions to optimize both models. The STVEN generator is firstly trained to reconstruct uncompressed videos from compressed ones and, independently, the rPPGNet estimator is optimized using high-quality videos. Finally, a joint training step is performed, fixing the parameters of the rPPGNet estimator and optimizing the STVEN generator to enhance facial videos for rPPG extraction.

In contrast to Yu et al., we propose a simpler two-stage approach that improves existing HR estimation in highly compressed scenarios by focusing solely on the physiological perspective. Our Pulse-Signal Magnification Network is designed to magnify rPPG characteristics in video rather than reconstructing all uncompressed video details, which are unnecessary for this task and make the model more difficult to train and less effective.

### III. METHODOLOGY

In this section, we introduce our proposed model, which is composed of the rPPG estimator and the Pulse-Signal Magnification network. Subsequently, we detail our two-stage training procedure and present our optimized objective function for rPPG recovery.

#### A. Problem formulation

Our framework aims to extract the rPPG signal from compressed videos by learning a suitable transformation of the video domain. This transformation aims to magnify the tiny pulse signal that is present in the video but has possibly been damaged or distorted by the compression algorithm. A key element for the success of our approach is to focus on restoring only the part of the video signal that is necessary to the rPPG estimation, but not the video as a whole, which would lead to a considerably more complex system.

Let  $\mathbf{C}^n = [c_1^n, c_2^n, \dots, c_T^n]$  be a facial compressed video  $n \in N_c$ , where  $N_c$  is the total number of compressed videos with the number of frames  $t \in T$  in our training set. The corresponding rPPG ground-truth signal from the compressed  $\mathbf{C}^n$  is denoted as  $\mathbf{y}_c^n = [y_{c,1}^n, y_{c,2}^n, \dots, y_{c,T}^n] \in \mathcal{Y}_c$  and it represents the pulse signal that we wish to extract from the video.

Given the above definitions, we denote our compressed rPPG video dataset as  $\mathcal{D}^c = [(\mathbf{C}^1, \mathbf{y}_c^1), \dots, (\mathbf{C}^{N_c}, \mathbf{y}_c^{N_c})]$ . Similarly, we assume that, during training, we have also access to another set of facial videos without compression<sup>3</sup>,  $\mathbf{U}^n = [u_1^n, u_2^n, \dots, u_T^n] \in \mathcal{U}$  with  $n \in N_u$ , where  $N_u$  is the total number of uncompressed videos, also with their corresponding PPG ground-truth  $\mathbf{y}_u^n = [y_{u,1}^n, y_{u,2}^n, \dots, y_{u,T}^n]$ , forming the rPPG uncompressed dataset  $\mathcal{D}^u = [(\mathbf{U}^1, \mathbf{y}_u^1), \dots, (\mathbf{U}^{N_u}, \mathbf{y}_u^{N_u})]$ .

As previously mentioned, our two-stage framework involves training two neural networks:  $f_\theta$  and  $m_\psi$ . The network  $f_\theta$  learns the mapping from uncompressed facial videos  $\mathcal{U}$  to rPPG signal  $\mathcal{Y}$ , while the network  $m_\psi$  maps the compressed RGB facial videos  $\mathcal{C}$  to a new pulse-signal magnification subspace  $\mathcal{M}$ :

$$\begin{aligned} f_\theta : \mathcal{U} &\rightarrow \mathcal{Y} \\ m_\psi : \mathcal{C} &\rightarrow \mathcal{M} \end{aligned} \quad (1)$$

where  $\theta$  and  $\psi$  refer to the rPPG and pulse-magnification network, respectively. Our objective is to partially approximate the relationship between uncompressed  $\mathcal{U}$  and compressed  $\mathcal{C}$  facial videos by learning a video transformation that effectively amplifies the information related to the pulse signal that was distorted by the compression effect:

$$\hat{\mathbf{y}}_M^n = f_\theta(m_\psi(\mathbf{C}^n)) \quad (2)$$

where  $\hat{\mathbf{y}}_M^n$  represents the rPPG signal estimated from pulse-magnified video, i.e. from the compressed facial video  $\mathbf{C}^n$  once it has been conveniently transformed into  $m_\psi(\mathbf{C}^n) \in \mathcal{M}$ . Notice that, in general,  $\mathcal{M} \neq \mathcal{U}$  except from the perspective of the recovered signal,  $\hat{\mathbf{y}}_M^n$ .

#### B. Networks Architecture

An illustration of the two networks previously described is provided in Figure 1. The rPPG estimator network  $f_\theta$  is a lightweight spatiotemporal model presented in [5]. This network effectively estimates rPPG spatiotemporal features by aggregating temporal derivative modules (TDM), emulating a

<sup>3</sup>It is also possible to use the same videos in set  $\mathcal{D}^c$  before compression, but this is not required.

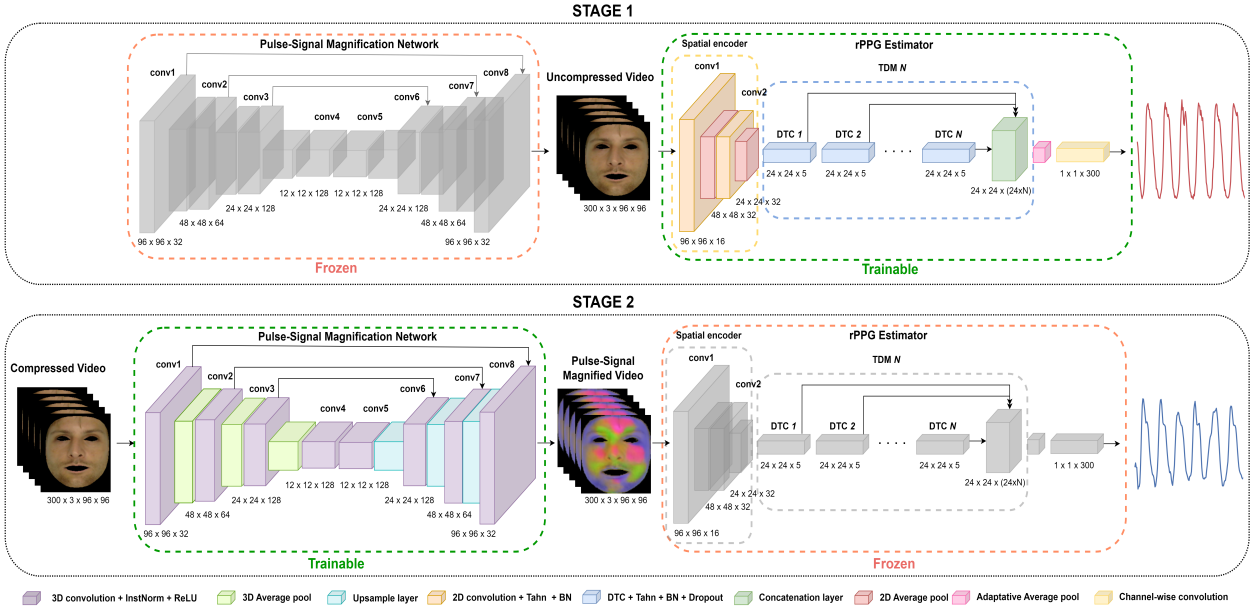


Fig. 1: Overall structure of our proposed model, which has two stages for rPPG recovery under compression. Firstly, the TDM model is trained on uncompressed data. Then, the Pulse-Signal Magnification network is trained on compressed data with fixed TDM model parameters.

Taylor series expansion. We selected this architecture because it achieves competitive results in current benchmarks while using fewer parameters than other alternatives with comparable performance.

The Pulse-Signal Magnification network  $m_\psi$  is an Unet-based network that learns the desired pulse-signal magnification transformation. This spatiotemporal network comprises three 3D convolutions with a 3x3x3 kernel, followed by ReLU activation functions, 3D instance normalization, and average pooling. We then employ two spatiotemporal convolutions in the lowest dimensionality space and reconstruct the latent space using three 3D upsampling convolutions. At each resolution level, we incorporate a skip connection to lead the network to produce the same facial data as the input.

### C. Two-stage Training Framework

The motivation for our proposed two-stage training framework is three-fold: 1) to better handle the domain gap between compressed and uncompressed videos in the recovery of remote PPG signal by magnifying the pulse signal in the video domain, 2) to leverage a pre-trained rPPG estimator network  $f_\theta$  on an uncompressed video dataset as a regularizer for the Pulse-Signal Magnification network  $m_\psi$ , and 3) to reduce the training complexity of the overall system. By decoupling the training into two stages, we can ensure that the Pulse-signal Magnification network  $m_\psi$  learns a representation that better approximates the performance of uncompressed videos.

#### 1) Stage I

The first stage of the framework consists of training our  $f_\theta$  as rPPG estimator from uncompressed data  $\mathcal{D}^u$ . This stage aims to obtain a pre-trained network that can estimate the PPG signal accurately from uncompressed videos, which can be used as a regularizer for the Pulse-Signal Magnification network  $m_\psi$  in the second stage. This stage is essential in

addressing the domain gap between compressed and uncompressed videos, as the pre-trained rPPG estimator network  $f_\theta$  can capture the signal from uncompressed videos more effectively than using compressed data. Therefore, the objective of this first stage is to optimize the  $f_\theta$  network over  $\theta$  parameters:

$$\min_{\theta} \frac{1}{N_u} \sum_{n=1}^{N_u} \mathcal{L}_{\text{rPPG}}(f_\theta(\mathbf{U}^n), \mathbf{y}_u^n), \quad (3)$$

where  $n$  is the index of the uncompressed video  $\mathbf{U}^n$ ,  $\mathbf{y}_u^n$  the corresponding PPG ground-truth signal, and  $\mathcal{L}_{\text{rPPG}}$  is the rPPG loss function that measures the difference between the estimated PPG signal and the PPG ground-truth signal, explained in Section III-D.

#### 2) Stage II

The second stage of the framework involves training a Pulse-Signal Magnification network  $m_\psi$  to learn an optimal video transformation. In a study by Nowara et al. [34], it was argued that training deep learning models with the same compression level as the testing data yields the best performance. Following this idea, the pre-trained rPPG estimator model  $f_\theta$  is designed to estimate the rPPG signal from non-compressed videos, while the Pulse-Signal Magnification network  $m_\psi$  learns to map videos in the domain of  $\mathcal{C}$  to a domain that magnifies the pulse-signal from compressed data  $\mathcal{D}^c$  so that it behaves like non-compressed data  $\mathcal{D}^u$ . In this way, it adapts the compression level of input data to the uncompressed format guided by the knowledge stored in the  $f_\theta$  network at Stage I.

Thus, the objective of the second stage is to jointly train both networks such that the output of  $m_\psi$  is regularized by  $f_\theta$ . The parameters  $\theta$  of the rPPG estimator network  $f_\theta$  are kept frozen during this training stage, i.e. only the parameters

$\psi$  of the Pulse-Signal Magnification network  $m_\psi$  are updated:

$$\min_{\psi} \frac{1}{N_c} \sum_{n=1}^{N_c} \mathcal{L}_{\text{rPPG}}(f_{\theta}(m_{\psi}(\mathbf{C}^n)), \mathbf{y}_{\mathbf{c}}^n), \quad (4)$$

where  $n$  is the index of the compressed video  $\mathbf{C}^n$ ,  $\mathbf{y}_{\mathbf{c}}^n$ , is the corresponding ground-truth PPG signal, and  $\mathcal{L}_{\text{rPPG}}$  is the rPPG loss function. In Section IV-C3, we will discuss the advantages of this two-step approach and present empirical evidence of its effectiveness in our experimental section.

#### D. Loss function

We use a combined loss function focused solely on the physiological aspect to guide the optimization of our model toward improving the pulse signal from the input video. The combined loss function comprises a temporal loss function aimed at restoring the intrinsic characteristics of the PPG waveform, and a frequency loss function, aimed at learning spectral features from the HR distribution.

For the temporal loss function, we adopt TALOS (Temporal Adaptive LOcation Shift) Loss, presented in [5] that allows training of deep learning methods invariantly to temporal offsets of the ground-truth signal, also known as Pulse Transit Time (PTT). Therefore, our  $\mathcal{L}_{\text{temp}}$  can be written as:

$$\mathcal{L}_{\text{temp}} = \sum_{k \in K} \text{MSE}(\hat{y}_t, y_{(t-k)}) \cdot p_{\theta}(k|s), \quad (5)$$

where the mean square error (MSE) is computed between the predicted rPPG signal  $\hat{y}_t$  and the ground-truth PPG signal  $y_{(t-k)}$  for each possible offset  $k$  and is weighted for each subject  $s$  according to the learned temporal-shift probability  $p_{\theta}(k|s)$ .

For the frequency loss function, we employ the signal-to-noise ratio (SNR) loss [8] to incorporate the HR estimation task as a classification problem in the frequency domain. Therefore, our  $\mathcal{L}_{\text{freq}}$  can be written as:

$$\mathcal{L}_{\text{freq}} = \text{CE}(\text{PSD}(\hat{y}_t), \text{HR}_{\text{gt}}), \quad (6)$$

where  $\text{CE}$  is the cross-entropy loss between the power spectral density  $\text{PSD}(\hat{y}_t)$  of the predicted rPPG signal  $\hat{y}$  and the HR ground-truth value,  $\text{HR}_{\text{gt}}$ .

In summary, the overall loss function  $\mathcal{L}_{\text{rPPG}}$  for both networks can be formulated as:

$$\mathcal{L}_{\text{rPPG}} = \mathcal{L}_{\text{temp}} + \lambda \cdot \mathcal{L}_{\text{freq}}, \quad (7)$$

where  $\lambda$  is a balancing parameter. In our experiments, we set  $\lambda = 0.01$  empirically based on our preliminary experiments.

#### E. Constrained Pulse-Signal Magnification space

Once our loss is formalized, let us revisit the concept behind our training stage II, introduced in Section III-C2. While the problem was initially described similarly to a video quality enhancement task, we do not actually target the restoration of the compressed video to obtain its uncompressed form, since there are no video reconstruction terms in our loss function. Instead, we only target the minimization of the estimated rPPG signal and the HR extracted from it, respectively, with  $\mathcal{L}_{\text{temp}}$  and  $\mathcal{L}_{\text{freq}}$ . This does not lead to the enhancement of the visual quality of the transformed video, but rather to its

transformation into an alternative, arbitrary domain  $\mathcal{M} \neq \mathcal{U}$  that is determined based on the aforementioned losses.

Thus,  $m_{\psi}(\mathbf{C}^n)$  is not a decompressed version of  $U^n$ , but the result of a transformation into a latent physiological domain in which the rPPG signal can be extracted with an accuracy similar to the uncompressed case, yet while starting from the compressed video input. As we shall see in the experiments, the transformed video is largely distorted in terms of visual quality, but it effectively focuses on the intensity changes that are relevant to estimate the rPPG signal. Indeed, after processing the input video with our Pulse-Signal Magnification network  $m_{\psi}$ , the pulsatile effect on the skin becomes magnified, to the extent that it can be appreciated by the naked eye, motivating the name of the method. This pulse-signal magnification space will be further analyzed in Section IV-C3.

## IV. EXPERIMENTS

In this section, we present the 4 benchmark datasets used in our experiments and describe the implementation and results of our method. We begin by examining the effect of the loss function, followed by investigating the impact of video compression on rPPG recovery using our baseline model. Next, we evaluate the performance of our two-stage model through intra-database and cross-database evaluations, showing its robustness to video compression. Finally, we present a comparison with existing rPPG approaches on compressed benchmarks.

### A. Datasets

We evaluate our approach on the following RGB video datasets.

The **UCLA-rPPG** dataset [59] comprises 489 videos from 98 subjects with diverse characteristics, including skin tone, ages, gender, and ethnicity. Each subject underwent 5 trials, with each trial lasting approximately 1 minute. The recordings were captured at a resolution of 640 x 480 pixels and 30 frames per second (FPS), in an uncompressed format, with an average bit rate of 295 Mb/s. Synchronous gold-standard PPG and HR measurements are provided alongside the facial videos. Due to the lack of predefined evaluation protocol in this dataset, we split the data ourselves into training (80%), validation (10%), and testing (10%) sets.

The **UBFC-rPPG** dataset [2] includes 42 RGB videos from 42 subjects. The recorded facial videos were acquired indoors with varying sunlight and indoor illumination at 30 FPS with a resolution of 640x480 in uncompressed 8-bit RGB format, with an average bit rate  $\approx 215$  Mb/s. PPG signal and heart rate at a sampling rate of 30 Hz are also provided. In our experiments, we use UBFC-rPPG in a cross-dataset evaluation, where all 42 videos are used for testing.

The **COHFACE** dataset [14] consists of 160 videos from 40 subjects, where each subject was recorded in 4 trials captured under two different lighting environments: studio and natural light. Each video was recorded at 20 FPS with a resolution of 640x480 for 1 minute and stored with heavy MPEG-4 compression, with an average bit rate  $\approx 0.25$  Mb/s. The physiological data consists of PPG and respiration ground-

truth signals with a sampling rate of 256 Hz. For our comparison, we follow the preassigned standard folds defined in the evaluation protocol for the dataset.

The **MAHNOB-HCI** dataset [45] includes 527 facial videos from 27 participants, with corresponding physiological signals. The videos were recorded at a resolution of 780x580 and 61 FPS, and were heavily compressed using the H.264/MPEG-4 AVC H.264/MPEG-4 AVC codec, with an average bit rate  $\approx$  4.20 Mb/s. Each recording contains several biosignals, from which we use the electrocardiogram (ECG) to extract the HR ground truth with the Bob Toolbox<sup>4</sup> [14]. To compare fairly with previous works [4], [19], [63], we use the standard 30-second clip (frames 306 to 2135) of each video.

## B. Implementation details

### 1) Preprocessing and training

We adopt the same preprocessing stage for each dataset in all our experiments. Firstly, we apply a facial segmentation to remove the background and non-skin areas adapting the Mediapipe Face Mesh<sup>5</sup> model [18]. This step reduces the complexity of video compression by focusing attention on the facial skin without introducing more complexity in terms of parameters or optimization tasks. Once the facial video is masked, each video frame is resized to  $96 \times 96$  pixels. The ground-truth bio-signal is preprocessed following [6] to denoise the raw PPG signal, which facilitates a better model convergence during training.

We implement our model using Pytorch 1.8.0 [38] and train it on a single NVIDIA GTX1080Ti. We use sequences of 300 frames with an overlap of 10 frames and use Adam optimizer with a learning rate of 0.0001 and weight decay of  $1e-5$ . In addition, when using the TALOS loss, we incorporate an extra SGD optimizer with a learning rate of 0.01 to optimize the parameters  $\theta^s$  of the temporal-shift distributions in Eq. (5). Finally, the estimated HR is computed from the predicted rPPG signal using the power spectral density (PSD). Before calculating the HR value, we apply a band-pass filter with cutoff frequencies of 0.66 Hz and 3 Hz.

### 2) Video compression settings

To evaluate the impact of video compression, we adopt the methodology from [30] for our ablation studies. Specifically, we produce compressed versions of the original uncompressed datasets by applying the H.264 codec with FFmpeg at various compression rates, categorized by the Constant Rate Factor (CRF). The CRF is a parameter that maintains a constant visual quality level by dynamically adjusting the bitrate based on video content complexity and ranges from 0 to 51, with lower values indicating higher quality. For our ablation studies, we consider CRF values of 0, 5, 10, 15, 20, and 25, with 0 representing the uncompressed data.

### 3) Metrics and evaluation

To evaluate the HR estimation performance we adopt the mean absolute HR error (MAE), the root mean squared HR error (RMSE) and Pearson’s correlation coefficients R, widely

used in the literature [23], [25]. For the UCLA-rPPG intra-dataset experiments, we use 300-frame sequences (10-second windows) without overlap for HR estimation. This approach is more challenging and informative compared to estimating HR based on the entire video sequence at once. For the remaining datasets, we compute whole-video performance given that most prior work follows that strategy. This allows for a direct comparison of our approach to several traditional and deep learning methods.

## C. Ablation studies

In Section II-B, we emphasized the importance of utilizing an uncompressed dataset for optimal results in our two-stage framework. As a result, we primarily choose the publicly available UCLA-rPPG dataset as the training dataset for our ablation studies. This dataset meets our criteria by including a substantial number of subjects with diverse skin types and being in an uncompressed format.

In this section, we present the results of our ablation studies on HR estimation. We conduct these studies using part of the UCLA-rPPG dataset for intra-dataset evaluation and the UBFC-rPPG dataset for cross-dataset evaluation. Firstly, we inspect the impact of the loss function on HR estimation using our baseline model. Next, we examine the effect of video encoding by applying different CRF values to recover the rPPG signal within the baseline model. Finally, we evaluate the performance of our proposed training procedure to mitigate the degradation introduced by video compression.

### 1) Impact of loss function

In this initial experiment, we evaluate the performance of the selected rPPG baseline, the TDM model [5], using different loss functions: TALOS as a temporal loss function, SNR loss as a frequency loss function, and the proposed combination of both, from Eq. 7. Table II presents the HR results of the TDM baseline for each loss function in both intra- and cross-dataset evaluations.

Based on the results, we notice that the TDM model yields better HR results when trained with the TALOS loss function ( $\mathcal{L}_{temp}$ ) as opposed to the SNR loss. However, during cross-dataset evaluation, we find that the SNR loss exhibits better generalization capabilities compared to the temporal loss. These outcomes align with the findings of Yu *et al.* [64], who highlight the challenges associated with training rPPG approaches using either temporal or spectral losses exclusively. The temporal loss offers advantages in extracting signal trend features, but it carries the risk of overfitting and limited generalization. Conversely, the SNR loss facilitates the learning of finer periodic features by leveraging the HR frequency bands but the presence of noise and the complexity of PPG waveforms can hamper the convergence of the model. Finally, we note that the combination of both losses produces a better performance than each one individually, similarly to [61], [64]. In the intra-database results, we appreciate almost the same performance combining both losses with respect to TALOS loss while in the cross-dataset evaluation, we observe a significant reduction of both MAE and RMSE compared with each of the losses individually, indicating

<sup>4</sup><https://www.idiap.ch/software/bob/>

<sup>5</sup>[https://github.com/google/mediapipe/blob/master/docs/solutions/face\\_mesh.md](https://github.com/google/mediapipe/blob/master/docs/solutions/face_mesh.md)

TABLE II: Impact of the loss function in HR measurement in intra-dataset and cross-dataset evaluation.

Loss function	Intra-dataset evaluation			Cross-dataset evaluation		
	UCLA-rPPG			UBFC-rPPG		
	MAE↓	RMSE↓	R↑	MAE↓	RMSE↓	R↑
$\mathcal{L}_{temp}$	1.00	4.43	0.90	2.54	6.18	0.93
$\mathcal{L}_{freq}$	1.16	4.51	0.89	2.38	5.91	0.94
$\mathcal{L}_{temp} + \mathcal{L}_{freq}$	1.02	4.45	0.90	1.66	5.54	0.95

better generalization ability. Thus, these results support our choice of the combined loss presented in Eq. 7.

### 2) Impact of video compression in HR estimation

In this section, we study the impact of the H264 encoding in the recovery of the rPPG signal using the TDM baseline model. To this end, we repeat the experiments from the previous section (keeping only the combined loss) but using increasingly compressed versions of the UCLA-rPPG and UBFC-rPPG datasets. Compression is applied to the whole dataset so that there is no compression mismatch between training and test sets. Table III summarizes the HR errors for different compression levels in terms of the CRF values.

For the intra-dataset evaluation, we observe a gradual increase in HR error as the compression rate increases. However, for CRFs between of 5 and 15, the HR error shows a rather minor increase with respect to the uncompressed baseline. Beyond a CRF of 20, we observe a significant rise in HR error. Such CRF values correspond to about 450 kb/s, which is 4 times lower than the bit rate at CRF 15 and about 655 times lower than the uncompressed video. The observed trend coincides with previous findings, which reported significant degradation of the rPPG signal beyond this CRF value, especially when the facial videos are downsampled [49].

In contrast to the intra-database evaluation, the cross-dataset evaluation shows a substantial increase in HR error, even for the smallest CRF levels. This indicates that, while the TDM baseline performs well with medium compression levels within the same database, it struggles to generalize effectively to different types of data, even when using the same compression level as the training set. This limitation can be attributed to the TDM model primarily capturing intrinsic temporal cues of rPPG through temporal derivatives, which are more sensitive to compression artifacts under mismatched conditions of the training and test data, such as motion or illumination. Nevertheless, to the best of our knowledge, we are the first to report the effect of different compression levels in cross-dataset experiments, hence this limitation might be shared by other data-driven models and not be exclusive of the TDM baseline.

### 3) Impact of network training procedure

We conduct an evaluation of the training procedure using two different strategies: *i*) the proposed two-stage training, and *ii*) end-to-end training. Differently from the previous two sections, in which only the TDM module was used, we now incorporate also the Pulse-Signal Magnification network, thus deploying our full system.

TABLE III: Impact of video compression for rPPG recovery in intra-dataset and cross-dataset evaluation.

CRF	Intra-dataset evaluation			Cross-dataset evaluation		
	UCLA-rPPG			UBFC-rPPG		
	MAE↓	RMSE↓	R↑	MAE↓	RMSE↓	R↑
0	1.02	4.45	0.90	1.66	5.54	0.95
5	1.12	4.52	0.90	3.14	7.26	0.91
10	1.18	4.58	0.89	4.57	12.33	0.77
15	1.26	4.69	0.89	6.75	14.74	0.71
20	1.94	7.25	0.76	12.82	21.83	0.49
25	2.98	9.33	0.72	14.44	24.5	0.43

Figure 2 depicts the evolution of HR errors using both strategies for the UCLA-rPPG and UBFC-rPPG datasets as a function of the compression level. When comparing the two strategies, it is evident that both yield competitive outcomes. However, the two-stage strategy demonstrates a lower HR error in both evaluations. Specifically, within the CRF range of 0 to 20, the two-stage procedure significantly reduces HR error compared to the end-to-end framework. This reduction helps mitigate compression degradation and achieves results similar to the uncompressed scenario. On the other hand, when the CRF is set to 25, both strategies experience an increase in HR error for both intra- and cross-dataset evaluation and their results become quite similar.

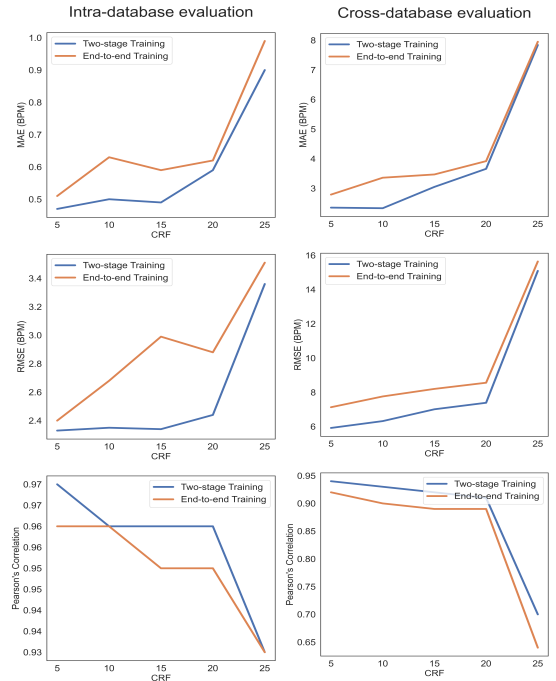


Fig. 2: Training procedure evaluation for rPPG recovery in intra-dataset and cross-dataset evaluation.

The superiority of the two-stage strategy in HR estimation can be explained by various factors. Firstly, in the end-to-end strategy, the network aims to recover the rPPG without any constraints related to the physiological nature of the signal. This increases the risk of overfitting, since the system must train a larger number of parameters at the same time and the function learned by each of the two composing blocks



is not necessarily the one expected by design. In contrast, the two-stage strategy employs a pre-trained TDM network that operates on uncompressed videos. This facilitates that the Pulse-Signal Magnification network (PSMN) learns a video transformation that focuses solely on enhancing the rPPG signal and directs attention exclusively to the regions of interest for rPPG. Hence, the initial training phase serves as a regularizer for the PSMN, ensuring pulse-signal magnification of the input data for extracting rPPG under conditions that match those from the initial pre-training dataset.

Independently of the training strategy, we can also analyze the impact of the PSMN by comparing the results in Figure 2 to those from Table III. Concretely, when using our PSMN, the error remains very similar to the uncompressed case (CRF = 0) for compressions up to CRF of 20, even for the cross-dataset evaluation, which was not the case when using just the TDM model. Beyond a CRF of 25, the HR error increases considerably, but it remains notably lower than the errors for the same CRF without the PSMN reported in Table III.

To gain a deeper understanding of the behavior of our proposed framework, Figure 3 provides a detailed example of the rPPG estimation using the two-stage strategy. The visualization reveals that the PSMN is learning a latent pulse magnification video transformation that highlights the facial regions relevant to rPPG extraction. Within this learned transformation, we can identify two prominent colors: green and magenta. These colors are predominantly distributed around the cheeks and forehead regions. Additionally, both in the generated video frames and the pixel evolution graph at the bottom of the figure, we can observe that the network learns opposing pulse patterns using these two colors, which are correlated to the cardiac cycle. Specifically, green regions are primarily activated during the systolic phase, whereas magenta regions are predominantly present during the diastolic stage.

#### 4) Evaluation on highly compressed datasets

After evaluating the training procedure on our ablation datasets, we also examine the performance of our approach on two highly compressed datasets: MAHNOB-HCI and COHFACE. Similarly to the previous sections, we use both cross-database and intra-database testing protocols.

For cross-database evaluation, we train on the UCLA-rPPG dataset compressed at the same rate as the test sets. Specifically, for the MAHNOB-HCI dataset we use the H.264 codec with a constant bit rate of 4200 kb/s while for the COHFACE dataset, we use the MPEG-4 codec with a constant bit rate of 250 kb/s. After compressing the UCLA-rPPG dataset, we use it to train our model and directly test on the MAHNOB-HCI and COHFACE datasets.

For intra-database evaluation on the MAHNOB-HCI, we initialize our model by pre-training on the compressed UCLA-rPPG dataset at 4200 kb/s and fine-tune it on the MAHNOB-HCI, following the subject-independent 9-fold cross-validation protocol introduced by Yu et al. [63]. Since there is no PPG signal for this dataset, we perform the fine-tuning considering just the SNR loss, which only requires HR estimates.

For intra-database evaluation in COHFACE, we initialize our model by pre-training on the compressed UCLA-rPPG dataset at 250 kb/s and fine-tune it on the COHFACE using its standard partition protocol [14]. Unlike the MAHNOB-HCI dataset, COHFACE contains PPG ground-truth data, allowing us to use the combined loss function introduced in Eq. 7.

Table IV summarizes the results. Firstly, we observe that the HR errors in the intra-dataset settings are excellent for both datasets, with the two-stage training slightly outperforming the end-to-end training on MAHNOB-HCI and more clearly in COHFACE. This highlights the ability of the PSMN to fine-tune the transformation of the input video to the characteristics of the targeted database. Particularly, the two-stage strategy

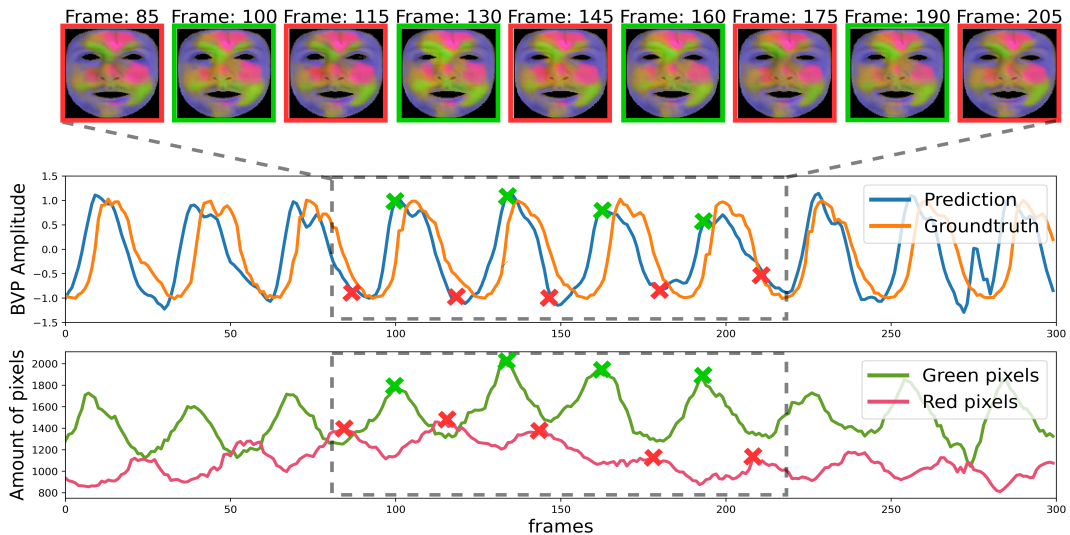


Fig. 3: Visualization of the learned video transformation for a sample compressed at CRF 15 from the UCLA-rPPG dataset. The top section displays the generated video,  $m_{\psi}(C^n)$  between frames 80 and 210. In the middle, we see the predicted rPPG and ground-truth signals. The bottom section shows the number of pixels over time for green and magenta colors, which are the dominant ones after the transformation and capture the blood pulse effect (see also the supplementary video).

TABLE IV: Evaluation of PSMN training procedures on highly compressed datasets.

Eval	Strategy	MAHNOB-HCI			COHFACE		
		MAE↓	RMSE↓	R↑	MAE↓	RMSE↓	R↑
Cross-Database	Two-stage	3.66	5.25	0.91	10.42	17.43	-0.07
	End-to-end	5.57	7.00	0.90	10.12	17.19	-0.04
Intra-Database	Two-stage	2.40	3.37	0.94	0.70	1.53	0.98
	End-to-end	2.41	3.49	0.93	0.86	2.66	0.96

exhibits impressive results on the COHFACE database, with 0.70 BPM (Beats Per Minute) MAE, 1.53 BPM RMSE, and 0.98 Pearson’s Correlation. These findings align well with the trends depicted in Figure 2, where intra-database results demonstrate competitive even at a CRF of 25, which is approximately equivalent to a bit rate of 250 kb/s used to encode COHFACE.

On the other hand, the cross-database errors are comparatively higher, but still at the top performance reported in the literature under comparable settings. For MAHNOB-HCI, the two-stage training is superior to the end-to-end approach as a result of the regularization effect of the pre-trained TDM. Nevertheless, this does not hold for the COHFACE dataset, in which neither of the strategies performs well under cross-database settings. We attribute this behaviour to the important differences in acquisition conditions between the UCLA-rPPG dataset and the COHFACE dataset.

#### D. Comparison with existing methods

In this section we compare our results to those reported by other methods on the COHFACE and MAHNOB-HCI datasets, which are two widely used benchmarks in HR measurement with high compression rates.

##### 1) Evaluation on MAHNOB-HCI dataset

Table V gathers the results reported in the literature for this database, separating them into intra- and cross-database settings to allow for a fair comparison. In terms of cross-database evaluation, our method achieves the best results, with a MAE of 3.66 BPM and an RMSE of 5.25 BPM, outperforming handcrafted methods and all deep learning approaches that report results in cross-database settings. Furthermore, our results outperform some learning-based approaches directly trained on the MAHNOB-HCI dataset, which can be attributed to our two-stage training procedure that allows the PSMN to learn an appropriate transformation for accurate rPPG estimation. By incorporating the TDM module, we add constraints that prevent the model from overfitting while effectively extracting meaningful rPPG features.

Under intra-dataset settings (i.e. fine-tuning on the MAHNOB-HCI dataset), we obtain notable improvement with respect to our cross-dataset results. The HR error reduces to 2.40 BPM for MAE, 3.37 for RMSE, and 0.94 for Pearson’s correlation. These results also outperform the current state-of-the-art approaches. Only the method by Jaiswal and Meenpa [17], which incorporates a color fusion technique to eliminate illumination artifacts, achieves similar results to ours, with slightly better MAE but slightly worse

TABLE V: Results of average HR estimation of MAHNOB-HCI.

Method	Cross-dataset eval			Intra-dataset eval		
	MAE↓	RMSE↓	R↑	MAE↓	RMSE↓	R↑
Poh2011 [41]	-	13.6	0.36	-	-	-
CHROM [8]	13.49	22.36	0.2	-	-	-
Li2014 [23]	-	7.62	0.81	-	-	-
SAMC [55]	4.96	6.23	0.83	-	-	-
HR-CN [50]	-	-	-	7.25	9.24	0.51
DeepPhys [4]	4.57	6.44	0.84	-	-	-
RhythmNet [33]	-	8.28	0.64	-	3.99	0.87
STVEN+rPPGNet [63]	-	-	-	4.03	5.93	0.88
STMap+CNN [47]	5.98	7.45	0.75	4.61	5.70	0.86
AutoHR [61]	-	-	-	3.78	5.10	0.86
Meta-rPPG [19]	-	-	-	3.01	3.68	0.85
PulseGAN [46]	4.15	6.53	0.71	-	-	-
rPPG-FuseNet [17]	-	-	-	<b>2.08</b>	3.41	0.92
PhysFormer++ [64]	-	-	-	3.23	3.88	0.87
<b>Proposed method</b>	<b>3.66</b>	<b>5.25</b>	<b>0.91</b>	2.40	3.37	<b>0.94</b>

RMSE and R. Interestingly, the results of STVEN+rPPGNet [63] yield significantly higher HR errors, despite of using a rather similar architecture to ours but targeting the enhancement of the entire video signal. This highlights the advantage of our approach, which focuses on restoring only the part of the video signal that is necessary to the rPPG estimation, facilitating training and improving performance.

##### 2) Evaluation on COHFACE dataset

The HR estimation results of the COHFACE dataset for existing methods using intra-dataset evaluation are presented in Table VI.

Specifically, our method shows similar HR MAE (0.70) to the best results reported to date, from the siamese-rPPG approach [54] but exhibits better RMSE (1.53 BPM) and R (approximately 0.98).

The effectiveness of our proposed two-stage framework, along with the incorporation of the PSMN, is showcased in Figure 4. This figure presents a comparison between the TDM baseline model and our proposed approach, using the ground-truth PPG signal from an especially difficult COHFACE sample under challenging illumination conditions. The results highlight how the Pulse-Signal Magnification approach significantly enhances the reliability and accuracy of the rPPG signal, surpassing the performance of the TDM baseline model.

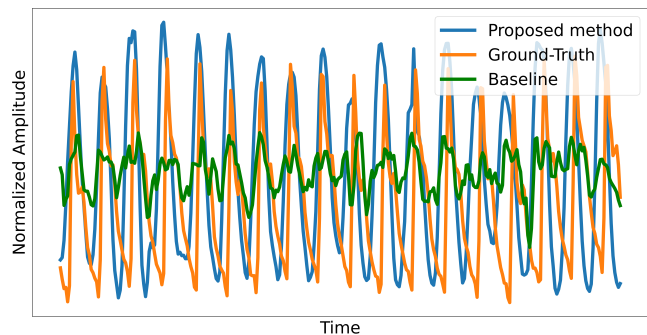


Fig. 4: Comparison of rPPG estimations between our baseline (green) and proposed model (blue) in the COHFACE dataset.

TABLE VI: Results of average HR estimation of COHFACE.

Method	MAE↓	RMSE↓	R↑
CHROM [8]	7.8	12.45	0.26
LiCVPR [23]	19.98	25.59	-0.44
Two stream [60]	8.09	9.96	0.40
HR-CNN [50]	8.1	10.8	0.29
Tsou2020 [54]	0.68	1.65	0.72
ETA-rPPGNet [16]	4.67	6.65	0.77
Gideon2021 [11]	1.5	4.6	0.90
TFA-PFE [21]	1.31	3.92	-
TDM [5]	2.48	5.90	0.81
<b>Proposed method</b>	<b>0.70</b>	<b>1.53</b>	<b>0.98</b>

## V. CONCLUSIONS

In this paper, we present a novel two-stage framework designed to mitigate the impact of video compression on remote HR measurement by enhancing and magnifying the video information required to estimate the rPPG signal. Our model consists of two sub-networks: an rPPG estimator and a Pulse-Signal Magnification network (PSMN). We present extensive evaluation on 4 public datasets and show that:

- 1) HR estimation from rPPG signals is strongly affected by compression. This is in line with numerous prior studies. We quantify the impact of various compression rates on the selected baseline model and datasets (Section IV-C2).
- 2) The introduction of the PSMN has a strong impact on HR estimation error, which is now robust against compression rates up to CRF = 20. Stronger compression levels do increase the HR estimation error, although considerably less than the baseline.
- 3) The proposed two-stage training outperforms the end-to-end alternative by a considerable margin, thanks to the regularization effect obtained by the rPPG estimator pre-training on uncompressed data (Section IV-C3).
- 4) The proposed optimization, exclusively from the rPPG perspective, yields a novel physiologically transformed video that amplifies the pulse signal, which would otherwise be imperceptible to the naked eye in the input RGB domain.
- 5) The proposed model can successfully adapt to datasets that are highly compressed and recorded in conditions that are quite different to those in the uncompressed pre-training data. The obtained results on the two most popular public datasets in such category show top state-of-the-art performance.

## ACKNOWLEDGMENTS

This work is partly supported by the eSCANFace project (PID2020-114083GB-I00) funded by the Spanish Ministry of Science and Innovation.

## REFERENCES

- [1] Y. Benezeth, P. Li, R. Macwan, K. Nakamura, R. Gomez, and F. Yang. Remote heart rate variability for emotional state monitoring. In *EMBS Int. Conf. Biomed. Health Inform. BHI*, pages 153–156. IEEE, 2018. 1
- [2] S. Bobbia, R. Macwan, Y. Benezeth, A. Mansouri, and J. Dubois. Un-supervised skin tissue segmentation for remote photoplethysmography. *Pattern Recognit. Lett.*, 124:82–90, 2019. 2, 3, 6
- [3] L. Cerina, L. Iozzia, and L. Mainardi. Influence of acquisition frame-rate and video compression techniques on pulse-rate variability estimation from vppg signal. *Biomed Tech (Berl)*, 64(1):53–65, 2019. 1, 3
- [4] W. Chen and D. McDuff. Deepphys: Video-based physiological measurement using convolutional attention networks. In *ECCV*, pages 349–365, 2018. 2, 7, 10
- [5] J. Comas, A. Ruiz, and F. Sukno. Efficient remote photoplethysmography with temporal derivative modules and time-shift invariant loss. In *CVPR*, pages 2182–2191, 2022. 4, 6, 7, 11
- [6] L. Dall’Olio, N. Curti, D. Remondini, Y. Safi Harb, F. W. Asselbergs, G. Castellani, and H.-W. Uh. Prediction of vascular aging based on smartphone acquired ppg signals. *Scientific reports*, 10:1–10, 2020. 7
- [7] A. Dasari, S. K. A. Prakash, L. A. Jeni, and C. S. Tucker. Evaluation of biases in remote photoplethysmography methods. *NPJ digital medicine*, 4(1):91, 2021. 2, 3
- [8] G. De Haan and V. Jeanne. Robust pulse rate from chrominance-based rppg. *IEEE Trans. Biomed. Eng.*, 60(10):2878–2886, 2013. 2, 6, 10, 11
- [9] C. Dong, Y. Deng, C. C. Loy, and X. Tang. Compression artifacts reduction by a deep convolutional network. In *ICCV*, pages 576–584, 2015. 1
- [10] J. R. Estep, E. B. Blackford, and C. M. Meier. Recovering pulse rate during motion artifact with a multi-imager array for non-contact imaging photoplethysmography. In *IEEE Trans. Syst. Man Cybern. Syst.*, pages 1462–1469. IEEE, 2014. 2, 3
- [11] J. Gideon and S. Stent. The way to my heart is through contrastive learning: Remote photoplethysmography from unlabelled video. In *ICCV*, pages 3995–4004, 2021. 11
- [12] A. Gudi, M. Bittner, and J. van Gemert. Real-time webcam heart-rate and variability estimation with clean ground truth for evaluation. *Applied Sciences*, 10(23):8630, 2020. 1, 3
- [13] S. Hanfland and M. Paul. Video format dependency of ppgi signals. In *Int. Conf. Electr. Eng. Inform. Commun. Technol.*, volume 1, 2016. 1, 2
- [14] G. Heusch, A. Anjos, and S. Marcel. A reproducible study on remote heart rate measurement. *arXiv preprint arXiv:1709.00962*, 2017. 2, 3, 6, 7, 9
- [15] G.-S. Hsu, A. Ambikapathi, and M.-S. Chen. Deep learning with time-frequency representation for pulse estimation from facial videos. In *IJCB*, pages 383–389. IEEE, 2017. 3
- [16] M. Hu, F. Qian, D. Guo, X. Wang, L. He, and F. Ren. Eta-rppgnet: Effective time-domain attention network for remote heart rate measurement. *IEEE Trans. Instrum. Meas.*, 70:1–12, 2021. 11
- [17] K. B. Jaiswal and T. Meenpal. rppg-fusenet: Non-contact heart rate estimation from facial video via rgb/msr signal fusion. *Biomed. Signal Process. Control*, 78:104002, 2022. 10
- [18] Y. Kartyunik, A. Ablavatski, I. Grishchenko, and M. Grundmann. Real-time facial surface geometry from monocular video on mobile gpus. *arXiv preprint arXiv:1907.06724*, 2019. 7
- [19] E. Lee, E. Chen, and C.-Y. Lee. Meta-rppg: Remote heart rate estimation using a transductive meta-learner. In *ECCV*, pages 392–409. Springer, 2020. 2, 7, 10
- [20] M. Lewandowska, J. Rumiński, T. Kocejko, and J. Nowak. Measuring pulse rate with a webcam—a non-contact method for evaluating cardiac activity. In *FedCSIS*, pages 405–410. IEEE, 2011. 2
- [21] J. Li, Z. Yu, and J. Shi. Learning motion-robust remote photoplethysmography through arbitrary resolution videos. In *AAAI*, volume 37, pages 1334–1342, 2023. 11
- [22] X. Li, I. Alikhani, J. Shi, T. Seppanen, J. Junttila, K. Majamaa-Voltti, M. Tulppo, and G. Zhao. The obf database: A large face video database for remote physiological signal measurement and atrial fibrillation detection. In *FG*, pages 242–249. IEEE, 2018. 2, 3
- [23] X. Li, J. Chen, G. Zhao, and M. Pietikainen. Remote heart rate measurement from face videos under realistic situations. In *CVPR*, pages 4264–4271, 2014. 2, 7, 10, 11
- [24] S. Liu, P. C. Yuen, S. Zhang, and G. Zhao. 3d mask face anti-spoofing with remote photoplethysmography. In *ECCV*, pages 85–100. Springer, 2016. 1
- [25] X. Liu, B. Hill, Z. Jiang, S. Patel, and D. McDuff. Efficientphys: Enabling simple, fast and accurate camera-based cardiac measurement. In *IEEE Winter Conf. Appl. Comput. Vis.*, pages 5008–5017, 2023. 2, 7
- [26] X. Liu, Z. Jiang, J. Fromm, X. Xu, S. Patel, and D. McDuff. Metaphys: few-shot adaptation for non-contact physiological measurement. In *CHIL*, pages 154–163, 2021. 2
- [27] H. Lu, H. Han, and S. K. Zhou. Dual-gan: Joint bvp and noise modeling for remote physiological measurement. In *CVPR*, pages 12404–12413, 2021. 2
- [28] E. Magdalena Nowara, T. K. Marks, H. Mansour, and A. Veeraraghavan. Sparseppg: Towards driver monitoring using camera-based vital signs estimation in near-infrared. In *CVPRW*, pages 1272–1281, 2018. 2, 3
- [29] D. McDuff. Deep super resolution for recovering physiological information from videos. In *CVPRW*, pages 1367–1374, 2018. 4

- [30] D. J. McDuff, E. B. Blackford, and J. R. Estepp. The impact of video compression on remote cardiac pulse measurement using imaging photoplethysmography. In *FG*, pages 63–70. IEEE, 2017. [1](#), [3](#), [7](#)
- [31] X. Niu, H. Han, S. Shan, and X. Chen. Synrhythm: Learning a deep heart rate estimator from general to specific. In *ICPR*, pages 3580–3585. IEEE, 2018. [2](#)
- [32] X. Niu, H. Han, S. Shan, and X. Chen. Vipl-hr: A multi-modal database for pulse estimation from less-constrained face video. In *ACCV*, pages 562–576. Springer, 2018. [2](#), [3](#)
- [33] X. Niu, S. Shan, H. Han, and X. Chen. Rhythmnet: End-to-end heart rate estimation from face via spatial-temporal representation. *IEEE TIP*, 29:2409–2423, 2019. [2](#), [3](#), [10](#)
- [34] E. Nowara and D. McDuff. Combating the impact of video compression on non-contact vital sign measurement using supervised learning. In *ICCVW*, pages 0–0, 2019. [1](#), [4](#), [5](#)
- [35] E. M. Nowara, D. McDuff, and A. Veeraraghavan. The benefit of distraction: Denoising camera-based physiological measurements using inverse attention. In *ICCV*, pages 4955–4964, 2021. [2](#)
- [36] E. M. Nowara, D. McDuff, and A. Veeraraghavan. Systematic analysis of video-based pulse measurement from compressed videos. *Biomed. Opt. Express*, 12(1):494–508, 2021. [1](#), [3](#), [4](#)
- [37] A. Pai, A. Veeraraghavan, and A. Sabharwal. Hrvcam: robust camera-based measurement of heart rate variability. *J. Biomed. Opt.*, 26(2):022707–022707, 2021. [3](#)
- [38] A. Paszke, S. Gross, F. Massa, A. Lerer, J. Bradbury, G. Chanan, T. Killeen, Z. Lin, N. Gimelshein, L. Antiga, et al. Pytorch: An imperative style, high-performance deep learning library. *Adv Neural Inf Process Syst*, 32, 2019. [7](#)
- [39] O. Perepelkina, M. Artemyev, M. Churikova, and M. Grinenko. Heart-track: Convolutional neural network for remote video-based heart rate monitoring. In *CVPRW*, pages 288–289, 2020. [2](#), [3](#)
- [40] M.-Z. Poh, D. J. McDuff, and R. W. Picard. Advancements in noncontact, multiparameter physiological measurements using a webcam. *IEEE Trans. Biomed. Eng.*, 58(1):7–11, 2010. [2](#)
- [41] M.-Z. Poh, D. J. McDuff, and R. W. Picard. Non-contact, automated cardiac pulse measurements using video imaging and blind source separation. *Optics express*, 18(10):10762–10774, 2010. [2](#), [10](#)
- [42] M. Rapczynski, P. Werner, and A. Al-Hamadi. Effects of video encoding on camera-based heart rate estimation. *IEEE Trans. Biomed. Eng.*, 66(12):3360–3370, 2019. [1](#), [3](#)
- [43] V. Ronca, A. Giorgi, D. Rossi, A. Di Florio, G. Di Flumeri, P. Aricò, N. Sciaraffa, A. Vozzi, L. Tamborra, I. Simonetti, et al. A video-based technique for heart rate and eye blinks rate estimation: A potential solution for telemonitoring and remote healthcare. *Sensors*, 21(5):1607, 2021. [1](#)
- [44] R. M. Sabour, Y. Benezeth, P. De Oliveira, J. Chappe, and F. Yang. Ufbc-phys: A multimodal database for psychophysiological studies of social stress. *IEEE Trans. Affect. Comput.*, 2021. [2](#), [3](#)
- [45] M. Soleymani, J. Lichtenauer, T. Pun, and M. Pantic. A multimodal database for affect recognition and implicit tagging. *IEEE Trans. Affect. Comput.*, 3(1):42–55, 2011. [2](#), [3](#), [7](#)
- [46] R. Song, H. Chen, J. Cheng, C. Li, Y. Liu, and X. Chen. PulseGAN: Learning to generate realistic pulse waveforms in remote photoplethysmography. *IEEE J.Biomed.Health Inform.*, 25(5):1373–1384, 2021. [2](#), [10](#)
- [47] R. Song, S. Zhang, C. Li, Y. Zhang, J. Cheng, and X. Chen. Heart rate estimation from facial videos using a spatiotemporal representation with convolutional neural networks. *IEEE Trans. Instrum. Meas.*, 69(10):7411–7421, 2020. [10](#)
- [48] J. Speth, N. Vance, A. Czajka, K. W. Bowyer, D. Wright, and P. Flynn. Deception detection and remote physiological monitoring: A dataset and baseline experimental results. In *IJCB*, pages 1–8. IEEE, 2021. [3](#)
- [49] R. Špetlík, J. Cech, and J. Matas. Non-contact reflectance photoplethysmography: Progress, limitations, and myths. In *FG*, pages 702–709. IEEE, 2018. [1](#), [2](#), [3](#), [8](#)
- [50] R. Špetlík, V. Franc, and J. Matas. Visual heart rate estimation with convolutional neural network. In *BMVC*, 2018. [2](#), [3](#), [10](#), [11](#)
- [51] R. Stricker, S. Müller, and H.-M. Gross. Non-contact video-based pulse rate measurement on a mobile service robot. In *RO-MAN*, pages 1056–1062. IEEE, 2014. [2](#), [3](#)
- [52] C. Takano and Y. Ohta. Heart rate measurement based on a time-lapse image. *Medical engineering & physics*, 29(8):853–857, 2007. [2](#)
- [53] H. E. Tasli, A. Gudi, and M. Den Uyl. Remote ppg based vital sign measurement using adaptive facial regions. In *ICIP*, pages 1410–1414. IEEE, 2014. [3](#)
- [54] Y.-Y. Tsou, Y.-A. Lee, C.-T. Hsu, and S.-H. Chang. Siamese-rppg network: remote photoplethysmography signal estimation from face videos. In *Proc.ACM Symp.Appl.Comput.*, pages 2066–2073, 2020. [10](#), [11](#)
- [55] S. Tulyakov, X. Alameda-Pineda, E. Ricci, L. Yin, J. F. Cohn, and N. Sebe. Self-adaptive matrix completion for heart rate estimation from face videos under realistic conditions. In *CVPR*, pages 2396–2404, 2016. [2](#), [10](#)
- [56] W. Verkrusse, L. O. Svaasand, and J. S. Nelson. Remote plethysmographic imaging using ambient light. *Optics express*, 16(26):21434–21445, 2008. [2](#)
- [57] W. Wang, A. C. den Brinker, S. Stuijk, and G. De Haan. Algorithmic principles of remote ppg. *IEEE Trans. Biomed. Eng.*, 64(7):1479–1491, 2016. [2](#)
- [58] W. Wang, S. Stuijk, and G. De Haan. A novel algorithm for remote photoplethysmography: Spatial subspace rotation. *IEEE Trans. Biomed. Eng.*, 63(9):1974–1984, 2015. [2](#)
- [59] Z. Wang, Y. Ba, P. Chari, O. D. Bozkurt, G. Brown, P. Patwa, N. Vaddi, L. Jalilian, and A. Kadambi. Synthetic generation of face videos with plethysmograph physiology. In *CVPR*, pages 20587–20596, 2022. [2](#), [3](#), [6](#)
- [60] Z.-K. Wang, Y. Kao, and C.-T. Hsu. Vision-based heart rate estimation via a two-stream cnn. In *ICIP*, pages 3327–3331. IEEE, 2019. [11](#)
- [61] Z. Yu, X. Li, X. Niu, J. Shi, and G. Zhao. Autohr: A strong end-to-end baseline for remote heart rate measurement with neural searching. *IEEE Sign. Process. Letters*, 27:1245–1249, 2020. [7](#), [10](#)
- [62] Z. Yu, X.-B. Li, and G. Zhao. Remote photoplethysmograph signal measurement from facial videos using spatio-temporal networks. In *BMVC*, 2019. [2](#)
- [63] Z. Yu, W. Peng, X. Li, X. Hong, and G. Zhao. Remote heart rate measurement from highly compressed facial videos: an end-to-end deep learning solution with video enhancement. In *ICCV*, pages 151–160, 2019. [1](#), [2](#), [4](#), [7](#), [9](#), [10](#)
- [64] Z. Yu, Y. Shen, J. Shi, H. Zhao, Y. Cui, J. Zhang, P. Torr, and G. Zhao. Physformer++: Facial video-based physiological measurement with slowfast temporal difference transformer. *IJCV*, 131(6):1307–1330, 2023. [2](#), [7](#), [10](#)
- [65] K. Zhang, W. Zuo, Y. Chen, D. Meng, and L. Zhang. Beyond a gaussian denoiser: Residual learning of deep cnn for image denoising. *IEEE TIP*, 26(7):3142–3155, 2017. [1](#)
- [66] Z. Zhang, J. M. Girard, Y. Wu, X. Zhang, P. Liu, U. Ciftci, S. Canavan, M. Reale, A. Horowitz, H. Yang, et al. Multimodal spontaneous emotion corpus for human behavior analysis. In *CVPR*, pages 3438–3446, 2016. [2](#), [3](#)
- [67] C. Zhao, W. Chen, C.-L. Lin, and X. Wu. Physiological signal preserving video compression for remote photoplethysmography. *IEEE Sens. J.*, 19(12):4537–4548, 2019. [1](#), [4](#)
- [68] C. Zhao, C.-L. Lin, W. Chen, and Z. Li. A novel framework for remote photoplethysmography pulse extraction on compressed videos. In *CVPRW*, pages 1299–1308, 2018. [1](#), [3](#), [4](#)